Malaysian Journal of Analytical Sciences (MJAS)



DFT STUDY ON STRUCTURAL PROPERTIES, DENSITY OF STATES AND BAND STRUCTURE OF MONOLAYER & BILAYER GRAPHENE

(Kajian Teori Tentang Sifat Struktur, Ketumpatan Keadaan dan Struktur Jalur Grafin Lapisan Tunggal dan Dwi Lapisan)

Nurhafizah Md Disa*, Henna Malakar, Nurhayati Abdullah

School of Physics, Universiti Sains Malaysia, 11800 USM Gelugor, Penang, Malaysia

*Corresponding author: mdnurhafizah@usm.mv

Received: 16 November 2021; Accepted: 27 February 2022; Published: 30 October 2022

Abstract

This two-dimensional (2-D) carbon structure, known as graphene, has tremendous potential due to its unique properties. This research intends to identify the existing knowledge gap because of the lack of substantial studies and prior comparisons in bilayer graphene and bring to light any pertinent differences between monolayer and bilayer graphene in this field. So, a density functional theory (DFT) study was done using a Quantum Espresso package for analysing the structural properties of mono- and bi-layer graphene. Generalised gradient approximation (GGA) under Perdew-Burke-Ernzerhof (PBE) of the DFT study and pseudopotential method was employed in this research. The monolayer and bilayer graphene have successfully predicted the bandgap and the Density of states (DOS), proving the zero-gap semiconductor tag. Furthermore, the band structure of the monolayer graphene illustrated a toroidal like shape, whereas the bilayer graphene projected a hyperbolic type of band-structure. The hybridisation of graphene was identified as sp² in which the bilayer graphene consumed more time for the orbital hybridisation compared to that of the monolayer. Therefore, this study is able to obtain the band gap vale for monolayer and bilayer graphene and provide a detail studies related to bilayer graphene beneficial for semiconductor applications.

Keywords: density functional theory, graphene, quantum espresso, structural properties, bandgap

Abstrak

Struktur karbon dua dimensi (2-D) ini, yang dikenali sebagai grafin, berpotensi besar kerana sifatnya yang unik. Penyelidikan ini mengatasi ketiadaan pengetahuan yang ada kerana kekurangan nilai teori yang signifikan dalam struktur jalur dwi lapisan dan perbandingan yang jelas dari lapisan tunggal dan lapisan dwi grafin dalam kajian sebelumnya. Oleh itu, kajian teori fungsi ketumpatan (DFT) dilakukan menggunakan pakej espresso kuantum untuk menganalisis sifat struktur grafin lapisan tunggal dan lapisan dwi. Kaedah gradien umum (GGA) di bawah Perdew-Burke-Ernzerhof (PBE) kajian DFT dan kaedah pseudopotensial digunakan dalam penyelidikan ini. Struktur jalur dan ketumpatan telah berjaya diramalkan oleh kajian grafin lapisan tunggal dan lapisan dwi, yang membuktikan tanda semikonduktor jurang sifar. Tambahan pula, struktur pita bentuk yang digambarkan untuk grafin lapisan tunggal adalah toroidal manakala grafin dwi lapisan mengunjurkan jenis struktur pita hiperbolik. Hibridisasi grafin dikenal pasti sebagai sp² di mana grafin dwi lapisan menggunakan lebih banyak masa untuk hibridisasi orbit berbanding dengan grafin lapisan tunggal. Oleh itu, kajian ini dapat memperoleh nilai jurang jalur untuk grafin lapisan tunggal dan dwi lapisan serta menyediakan kajian terperinci berkaitan grafin dwilapisan yang bermanfaat untuk aplikasi semikonduktor.

Kata kunci: teori fungsi ketumpatan, grafin, espresso kuantum, sifat struktur, jurang jalur

Nurhafizah et al.: DFT STUDY ON STRUCTURAL PROPERTIES, DENSITY OF STATES AND BAND STRUCTURE OF MONOLAYER & BILAYER GRAPHENE

Introduction

Carbon-based materials have advanced at a breakneck pace over the last few decades, particularly in the previous decade. For instance, carbon nanotubes, carbon nanofibers, graphene and carbon sponges [1] are carbonbased materials. The fullerene discovery, the carbon nanotubes, and the graphene have dramatically increased the variety of carbon-based materials available to researchers. The critical experiments of Novoselov and Geim in isolating graphene and identifying its basic properties sparked a surge in interest in graphene [2]. Graphene, as mentioned previously, is a carbon nanomaterial of zero-bandgap [3-4], a planar two-dimensional (2-D) hexagonal lattice [5-14], and sp2 bonded carbon atom [8, 15-17]. These carbon atoms are bound to the of their neighbours in the graphene lattice by σ bonds. The particles in the lattice each have a π orbital [18], which helps form an independent electron network. Graphene has strong electrical conductivity[5, 6, 8, 10-12, 14, 16, 19, 20], because of freedom of the π electrons in 2-D plane of a graphene sheet.

Electron transfer occurs at room temperature and below, resulting in low resistance and high conductivity due to the material's unique band structure [21]. It is said that a two-dimensional (2-D) sheet of crystals is entirely stable, as it is slightly wavy rather than flat. The highexpanded surface area [4, 5, 7, 16, 21-22], electrical conductivity [5, 6, 8, 10-12, 14, 16, 19-20], highvelocity and high absorption rate[23] of graphene add to each other to yield a lot of these properties. To top it all of this, it also has exceptional electrical properties such as low noise and high mobility [5, 7, 9, 21, 24-25]. Great attention has recently been directed toward electronic devices such as biosensors [6, 7, 12, 15], radio frequency (RF) transistors [6], and flexible displays. Aside from this, graphene has a wide range of possible uses in electronics, optical, photonics, and technologies such as electrochemical energy storage [3]. Due to its unique physical properties, monolayer and bilayer graphene-based quantum electronic devices are in-demand today [26]. DFT is very accurate in predicting atomic structures, properties and phonon spectrums [27]. Several interpretations of good accordance between DFT simulations and observational study demonstrate that DFT is highly appropriate and precise for infinitesimal investigations of physics and chemistry. Knowledge of density of states and electronic bandgap is valuable when modelling materials for

energy applications, such as graphene.

The experimental value of monolayer graphene from the study of Jeon et al. is reported to be 0.2eV [28]. Zhang and Quhe et al. have found the experimental value of band gap for bilayer graphene and is said to be 0.25eV [29-30]. To investigate the properties of a finite-size graphene sheet, Banerjee et al. experimented with various possible defects and edge effects and used software such as MOLDEN and GAMESS-US [31]. However, this software can be used for generating the molecular and electronic structure only, unlike Quantum Espresso that can calculate the structural and other electrical properties of graphene. Besides, Abbood and co-workers [32] used Gaussian 09 package to study electronic and electrical graphene sheets. Gaussian software utilises local basis functions rather than planewave to compute them, so it is more challenging to find basis functions.

In a study done by Geng and co-workers, DFT calculations using CASTEP software was utilised to evaluate the DFT aspects of the interface between graphene and ZnO [33]. Zhu and co-workers also used CASTEP software to study the electronic properties of nano-structural ZnO [34]. Although CASTEP can be used as one of the DFT studies, it has drawbacks at the price as it is licensed software, unlike Quantum Espresso (OE), an open-source code. OE is an open-source quantum mechanical software package with high performance capable of supporting various applications at the nanoscale level, including the design of materials, structural optimisation, and the simulation of atomic electronic structures, all based on DFT theory. The past research proves that Quantum Espresso is the best for studying and analysing the properties of graphene sheets among the other software. Pashangpour and co-workers also used Quantum Espresso to investigate the structural and electronic properties while adhering to Density Functional Theory (DFT) [35]. However, his study has not discovered the value of the bandgap for monolayer and bilayer graphene (AA or AB stacking).

Investing substantial time over the years has taken place to enhance the Quantum Espresso distribution by advancing computational methods, theoretical studies, and property calculations and improving interoperability with external codes [36]. High performance was one of the main motivations behind the Quantum Espresso project's inception [37]. Past research proves that Quantum Espresso is the best for studying and analysing the properties of graphene sheets among the other software. However, detailed studies of monolayer and bilayer graphene are not discovered using Quantum Espresso. Therefore, this research attempts to do detailed studies on monolayer and bilayer graphene using the DFT study with the Quantum Espresso package.

Computational Details

Density Functional Theory (DFT) [38-44] and the generalised gradient approximation (GGA) known as Perdew-Burke-Ernzerhof (PBE) were used in the PWSCF code to obtain the first-principles calculations. The input files are created using PW Graphical User Interface (GUI) in Quantum Espresso software package under Linux 64-bit. Kohn Sham orbitals are expanded in a plane-wave basis set. Norm-conserving (NC) and ultra-soft (US) forms make up most of the pseudopotentials used in plane-wave electronic structure codes. Thus, this allows for a much lower cut-off in the basis set, which results in a much better cut-off, faster computational efficiency and increased accuracy. Fermidistribution smoothing was performed using a Monkhorst & Pack ($10 \times 10 \times 1$) particular point grid used to perform Brillouin zone integrations, using Gaussian smearing technique with a smearing width of 0.01 Rydberg (Ry).

For monolayer graphene, the energy cut-off (80Ry) and the charge density (320Ry) are set, while for bilayer graphene, these values are 40Ry and 225Ry, respectively. With the ultra-soft pseudopotential of

bilayer graphene, using lower cut-off energy is preferable. Variable cell relaxation calculation was done to obtain the optimised cell lattice vectors by introducing Broyden-Fletcher-Goldfarb-Shanno (BFGS) algorithm as the type of ion dynamics. Relaxation calculation was also performed to get the optimised atomic coordinates essential for other following calculations. Burai Software, a GUI for Quantum Espresso (QE) was used to obtain the unit cell and lattice structure of monolayer and bilayer graphene.

K points were chosen to be automatic for Self-Consistent Field (SCF) and non-SCF calculations, whereas k points were set to 'crystal b' for band calculations. To calculate the density of states (DOS) calculation, grids of $(24 \times 24 \times 1)$ and $(11 \times 11 \times 3)$ for monolayer and bilayer graphene, respectively, were used using non-self-consistent field type. The number of bands was set to be 8 for monolayer graphene whereas 16 for bilayer graphene. Another feature of Brillouin zone is that they have been fine-tuned to obtain band structure. XCRYSDEN was used to find paths along the primitive Brillouin zone using k-path selection. After locating symmetrical points on the selection set, the symmetrical points are used for the band calculation. The selected high symmetrical points are tabulated in Table 1 and Table 2 for monolayer and bilayer graphene, respectively. The Quantum Espresso software package computed the bandgap, highest occupied molecular orbital (HOMO), lowest unoccupied molecular orbital (LUMO), and Fermi energy. In order to obtain information about the orbitals, the projected band structure calculation was done.

Table 1. Coordinates values for Brillouin zone (Monolayer)

Coordinates	Х-	y -	Z-
K	0.33	0.33	0
L	0	0	0
M	0.5	0	0

Table 2. Coordinates values for Brillouin zone (Bilayer)

			<u> </u>
Coordinates	х-	y -	Z-
A	0	0	0
Н	0.67	0	0
K	0.67	0	0
L	0.5	0.29	0.14
M	0.5	0.29	0

Result and Discussion

Structural properties

Monolayer and bilayer graphene atomic geometries are optimized as the initial step. This type of calculation is done so that other analysis uses these optimized atomic coordinates, which is beneficial for less or defect-free structure and structural optimization. The bond length between C-C is 1.4214Å which is in excellent agreement with the experimental value of bond length 1.42 Å [45], and the bond angle of C-C-C is 120°. The unit cell and hexagonal lattice structure in 2-D and 3-D viewed in XCRYSDEN for monolayer graphene and bilayer graphene are illustrated in Figure 1 and Figure 2, respectively. The unit cell of monolayer graphene contains two carbon atoms, whereas four carbon atoms are reported to be for bilayer graphene with a lattice constant of 2.467 Å. The AB bilayer is 3.35 Å apart, which is in the range of interlayer distance by past researchers [46-47]. In addition, the shape of the unit cell of monolayer and bilayer graphene is said to be in a lozenge shape. The lattice structure of the monolayer can be seen to be as a single layer of atoms with the axis of direction given in Figure 1(b) & (d). Therefore, these structures are proven accordingly as monolayer graphene, which is in excellent agreement with the experimental design [48]. The lattice structure of the bilayer can be seen to be stacked up as double or two layers of atoms with the axis of direction given in Figure 2(b) & (d). Therefore, these structures are verified

accordingly as bilayer graphene, which is in excellent agreement with the experimental design [49]. In AB bilayer graphene, half of the carbon atoms in the upper layer are located above the centres of the lower-layer hexagons. AB bilayer graphene is the most stable [50], and it has a wide range of applications because of its stable characteristics.

The charge density of graphene is visualized under Visualization for Electronic & Structural Analysis (VESTA) software illustrated in Figure 3. Color in the 4 edges of this figure refers to electrostatic potential, where green represents positive charge and orange represents negative charge. The arrow in Figure 3 indicates the yellow color in the unit cell, indicating graphene's charge density. The charge distribution is equally transmitted in the graphene unit cell, implying a minimal structure defect. The output file details are tabulated in Table 3, in which the input file of PP.X was used for data analysis and plotting purposes. The space group of the graphene is P1, where P indicates primitive lattice type and the symbol P 1 refers to triclinic Bravais lattice. The lattice constant is in excellent agreement with the theoretical value of 2.47 Å [42]. The grid size was changed from a smooth grid of (10 x 10 x 1) to a denser grid of (27 x 27 x 216) to view the charge density. Dense grids of k-points are needed for periodic structures.

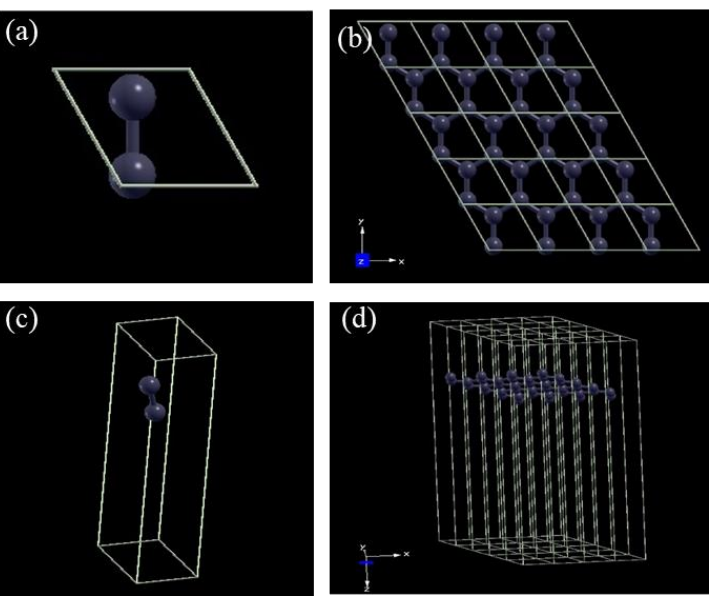


Figure 1. Monolayer graphene unit cell (a) 2-D (c) 3-D (b) and lattice structure (b) 2-D (d) 3-D

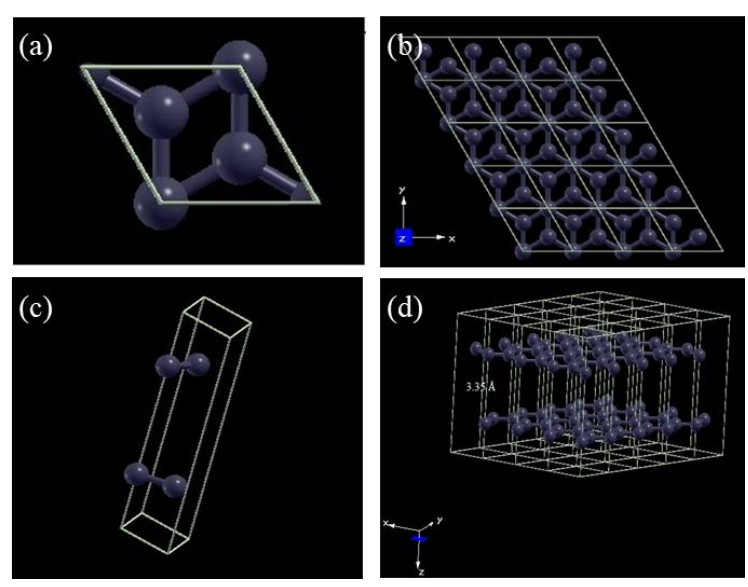


Figure 2. Bilayer graphene unit cell (a) 2-D (c) 3-D (b) and lattice structure (b) 2-D (d) 3-D

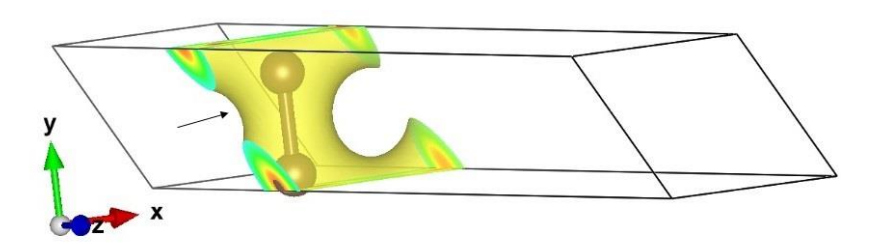


Figure 3. Charge density of graphene

Table 3. Structural details of the unit cell of graphene

Space Group	Lattice Constant, Å	Bond Length, Å	Angle	Grid Size $(x \times y \times z)$	Volume, Å ³
	A = 2.4674		$\alpha = 90.0^{\circ}$		
P1	A = 2.4674	1.4214	$\beta = 90.0^{\circ}$	$27 \times 27 \times 216$	104.1362
	C = 20.000		$\gamma = 120.0^{\circ}$		

Electronic properties (density of states)

The density of states represents the number of electron states per unit volume per unit energy. In DOS calculation, the type of calculation used was non-SCF. The solution field minimizes the density charge functional until a predefined limit in the energy difference between two consecutive steps. The non-SCF analysis used a denser grid $(24 \times 24 \times 1)$ for monolayer graphene and a grid $(11 \times 11 \times 3)$ for bilayer graphene. Grid size here indicates the lattice size. *nbnd* is specified

in this type of calculation, and it represents the number of bands where electron value 8 and 16 is included for monolayer and bilayer graphene respectively. The Brillouin zone is divided into a tetrahedron. The energies of the corners of each tetrahedron are used to calculate the eigen energies. These values are then interpolated to obtain the overall eigen energy. It follows the trapezoidal rule for approximating the integral of single-variable functions, making the tetrahedron method similar. Therefore, the type of occupation was

set to 'tetrahedra' as this is applicable for accuracy in non-SCF calculation. Figure 4 and Figure 5 illustrate the density of states (DOS) for mono- and bi-layer graphene.

The Fermi energy was set to zero in the axis. It can be interpreted from those figures, the DOS is near 0, around the energy of 0. Since the cones are connected at an infinitely small point with no range or extent in the E-k space of band structure, the density of states is 0 for both monolayer and bilayer graphene. Therefore, there are no states at this point, so DOS is zero. In other words, we can say that the DOS of graphene increases linearly with energy. The bilayer graphene also shows zero DOS because layers' stacking (AB) is through planes and not edges in this study. Figure 6 shows the shapes formed by the bonds between carbon atoms (edge stacking pattern).

AB stacking of bilayer used in this research is of one structure only, which is zigzag pattern similar to plane AB stacking. The AB stacking of bilayer through armchair or zigzag nanoribbons (narrow strips of graphene) has specific DOS and bandgap because it depends on the edge orientation. This value is due to the stacking of layers through edges which can modify the electronic properties of graphene. For instance, in the armchair pattern, the bandgap is dependent on the nanoribbon width, unlike the zigzag pattern. The zigzag structure supports localized states [51-52], resulting in covalent bond formation, bonding and anti-bonding states. Moreover, the zigzag pattern, similar to plane AB stacking, possesses metallic behavior regardless of graphene nanoribbon width [53]. Consequently, the DOS and band gap is still zero for the zigzag pattern. To study the edge stacking in bilayer graphene, LDA should be used. However, GGA was used in this study instead of LDA because GGA gives a minor error and is more accurate in illustrating structural or electronic properties. LDA underestimate the bond length and over-bind, which causes a more significant interatomic force constant (IFC) to be generated [54].

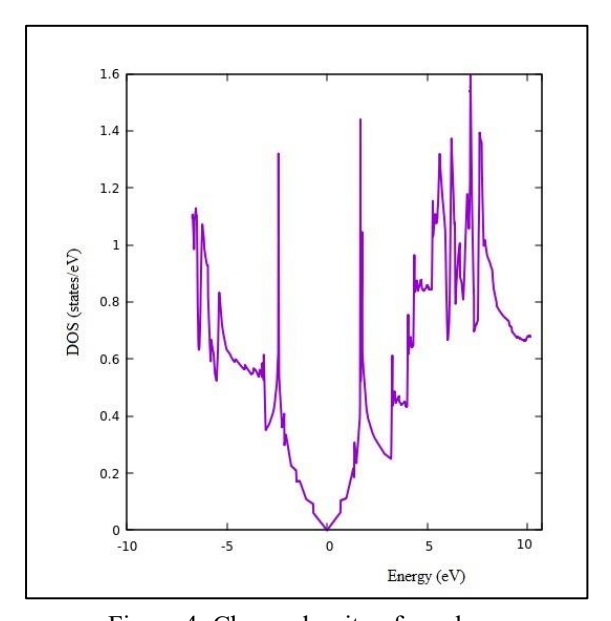


Figure 4. Charge density of graphene

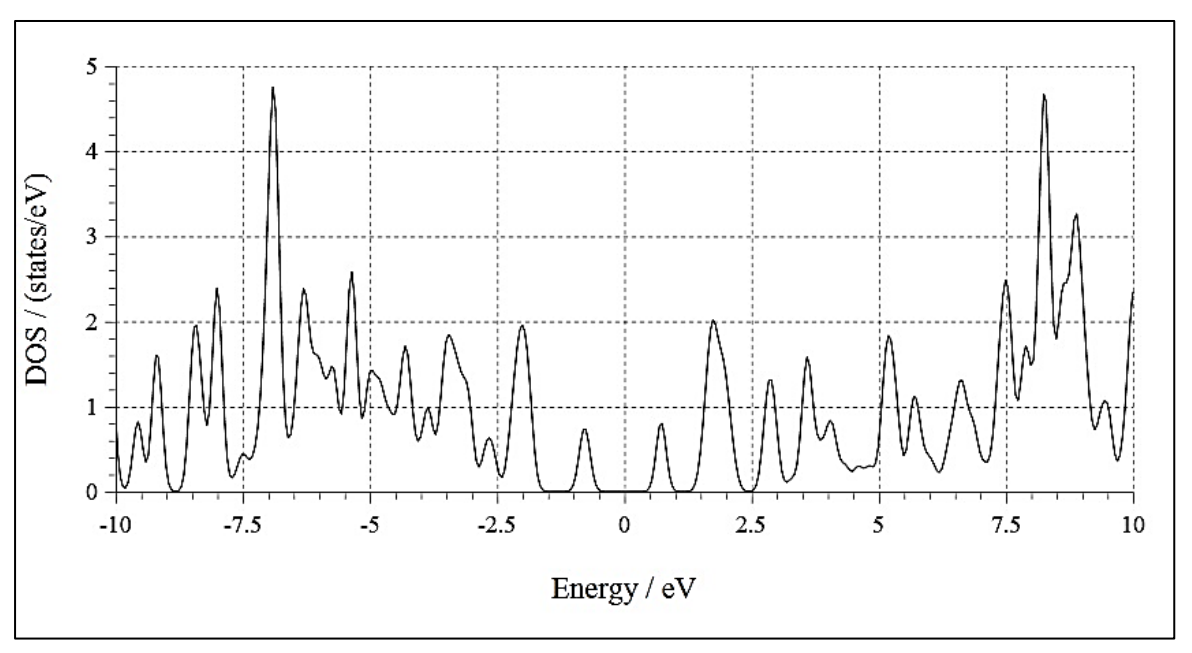


Figure 5. Density of states (DOS) of bilayer graphene

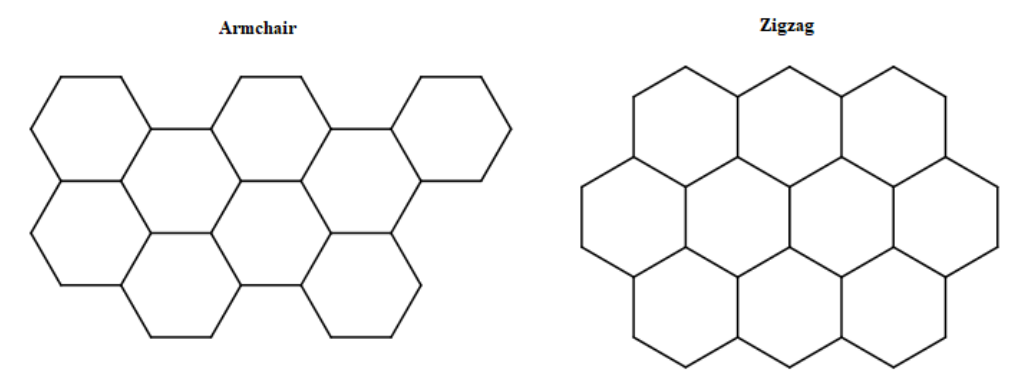


Figure 6. Shapes formed by the bonds between carbon atoms (edge stacking pattern)

Electronic properties (projected band structure)

The results obtained from the projected band structure are illustrated in Figure 7 for monolayer graphene and Fig. 8 for bilayer graphene, respectively. Two and four

atoms were specified for monolayer and bilayer graphene, respectively, based on their unit cell. Therefore, the monolayer has eight atomic states, and the bilayer has sixteen atomic states.

- a) l = 0 indicates the s orbital
- b) l = 1 refers to the p orbital
- c) m=-1,0,1 refers to the magnetic quantum number $(p_x\,,p_y\,,p_z)$

Nurhafizah et al.: DFT STUDY ON STRUCTURAL PROPERTIES, DENSITY OF STATES AND BAND STRUCTURE OF MONOLAYER & BILAYER GRAPHENE

The results projected in Figure 7 and Figure 8 concludes that graphene has s and 2p orbitals. The total charge in Figure 8 and Figure 10 for monolayer and bilayer graphene recorded 4.0497 and 3.9553, which gives a value of 4.0 when rounded off to one decimal place. This total charge here represents the number of valence electrons. The spilling parameter setting represents what percentage of the total density is not projected by these schematics. As the spilling parameter gets closer to zero, the representation is more accurate. Therefore, both mono- and bi-layer graphene recorded a value of 0.01, which is in excellent agreement with the accuracy range. Carbon with 6 electrons has 1s², 2s², 2p² ground-state electron configuration, whereby two is in the inner shell, and four are in the outer shell. In graphene, each carbon atom is connected to three other carbon atoms on the two-dimensional plane, leaving one outer shell electron available for chemical bonding. Carbon atoms in graphene have sp² hybridized, which means the mixture of a single 2s orbital with two 2p orbitals. The diagram in Figure 9 is the representation of sp² hybridization with 120° spacing. Therefore, the orbitals (2s, $2p_x$, $2p_y$) results in trigonal planar (120° apart) structure with the formation of σ bond between carbon atoms. Because of this arrangement, the hexagonal structure of graphene was formed. Carbon's robust lattice structure is due to the σ bond. Since the Pauli principle is in effect, these bands have a filled shell. A valence band is therefore formed. p_zorbital covalently bound to carbon atoms occurs along the graphene plane [55]. This p_z orbital constitutes the π bond. When joining together, the π bonds form the π band (bonding) and π^* bands (antibonding). The π band is half-filled since every p orbital contains one extra electron and is not doped [50]. Most graphene's remarkable electronic properties are credited to these bands because they have a half-filled band that enables free-moving electrons. Because bilayers are hybrids between s orbitals and p_z orbitals, the hybridization is more time-consuming than for monolayer graphene. Therefore, the hybridization for bilayer graphene is more complicated than monolayer graphene.

Besides, the highest occupied molecular orbital (HOMO) and lowest unoccupied molecular orbital (LUMO) can provide information on the chemical stability [56-58]. The gap between the highest energy HOMO and LUMO orbitals is where most likely excited states can be found. Therefore, it is crucial to know the energy gap. Conjugated π orbital systems allow for the transfer of energy more freely within a molecule, helping to keep it stable. Better molecular stability is associated with higher HOMO-LUMO gaps. Monolayer and bilayer graphene have recorded values of 2.034eV and 1.877eV, respectively, for (HOMO - LUMO) gap. Consequently, monolayer graphene is more stable molecularly in this study. HOMO - LUMO gap value from theoretical study reported to be in range of 2.2eV to 3.1eV for graphene quantum dot [59]. However, there's no value reported in experimental study for monolayer and bilayer graphene.

```
(a)
         state #
                      1: atom
                                   1 (C ), wfc 1 (l=0 m= 1)
         state #
                      2: atom
                                   1 (C ), wfc 2 (l=1 m= 1)
         state #
                                          ), wfc 2 (l=1 m= 0)
                      3: atom
                                   1 (C
                                          ), wfc 2 (l=1 m= -1)
         state #
                      4: atom
                                   1 (C
                                   2 (C
                                          ), wfc 1 (l=0 m= 1)
         state #
                      5: atom
         state #
                      6: atom
                                   2 (C ), wfc 2 (l=1 m= 1)
         state #
                      7: atom
                                   2 (C
                                         ), wfc 2 (l=1 m= 0)
                      8: atom
                                   2 (C ), wfc 2 (l=1 m=-1)
         state #
                                       (b)
Lowdin Charges:
           1: total charge =
                            4.0497, s = 0.8933,
           1: total charge = 4.0497, p = 3.1564, pz= 1.0799, px= 1.0458, py= 1.0307,
    Atom # 2: total charge = 4.0497, s = 0.8933,
    Atom # 2: total charge = 4.0497, p = 3.1564, pz= 1.0799, px= 1.0458, py= 1.0307,
    Spilling Parameter: 0.0124
              Figure 7. Monolayer graphene (a) atomic states (b) lowdin charges
                                       (a)
                           1: atom
                                    1 (C ), wfc 1 (1=0 m= 1)
                  state #
                                    1 (C ), wfc 2 (1=1 m= 1)
                  state #
                           2: atom
                  state # 3: atom
                                   1 (C ), wfc 2 (1=1 m= 0)
                  state \# 4: atom 1 (C ), wfc 2 (l=1 m= -1)
                  state # 5: atom 2 (C ), wfc 1 (1=0 m= 1)
                  state # 6: atom 2 (C ), wfc 2 (l=1 m= 1)
                  state # 7: atom 2 (C ), wfc 2 (l=1 m= \theta)
                  state # 8: atom 2 (C ), wfc 2 (1=1 m= -1)
                  state # 9: atom 3 (C ), wfc 1 (l=0 m= 1)
                  state # 10: atom 3 (C ), wfc 2 (1=1 m= 1)
                  state # 11: atom 3 (C ), wfc 2 (l=1 m= 0)
                  state # 12: atom 3 (C ), wfc 2 (l=1 m= -1)
                  state # 13: atom 4 (C ), wfc 1 (l=0 m= 1)
                  state # 14: atom 4 (C ), wfc 2 (l=1 m= 1)
                  state # 15: atom 4 (C ), wfc 2 (1=1 m= 0)
                  state # 16: atom 4 (C ), wfc 2 (1=1 m= -1)
                                       (b)
 Lowdin Charges:
            1: total charge = 3.9553, s = 0.9179,
           1: total charge = 3.9553, p = 3.0374, pz= 0.9879, px= 1.0247, py= 1.0247,
     Atom #
           2: total charge = 3.9553, s = 0.9179,
           2: total charge = 3.9553, p = 3.0374, pz= 0.9879, px= 1.0247, py= 1.0247,
     Atom #
            3: total charge = 3.9565, s = 0.9180,
     Atom #
            3: total charge =
                             3.9565, p = 3.0385, pz= 0.9888, px= 1.0248, py= 1.0248,
            4: total charge =
                             3.9565, s = 0.9180,
     Atom # 4: total charge = 3.9565, p = 3.0385, pz= 0.9888, px= 1.0248, py= 1.0248,
     Spilling Parameter:
                       0.0110
```

Figure 8. Bilayer graphene (a) atomic states (b) lowdin charges

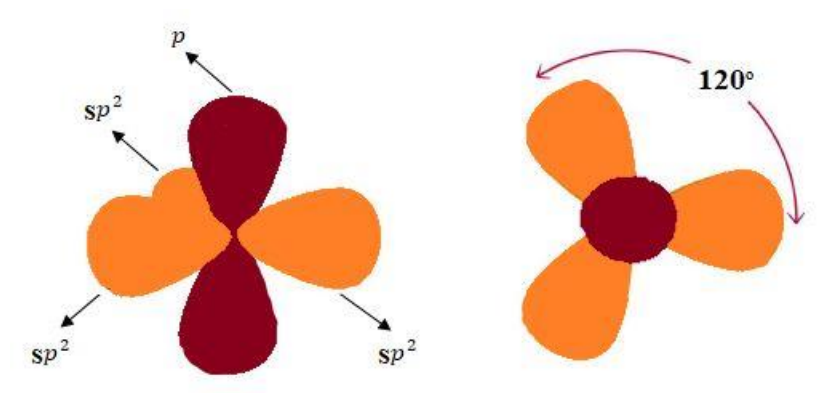


Figure 9. sp² hybridization of carbon in graphene b.) trigonal planar with 120° apart

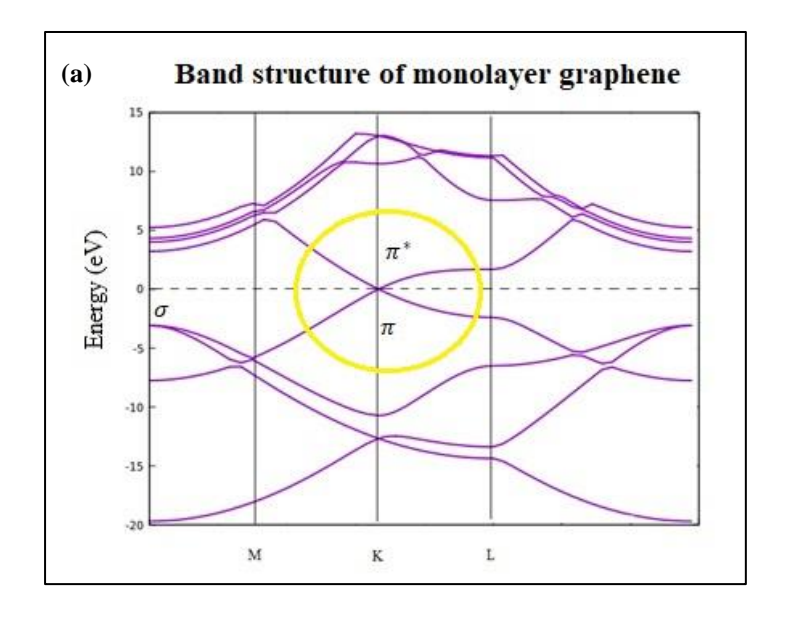
Electronic properties (band structure)

Figure 10 illustrates band structure for monolayer and bilayer graphene obtained from the band calculation explained in methodology. The band structure where two cones touching at the Dirac point is presented in Figure 11. The dispersion of the bands can be visualized from the result as two cones that intersect at the Dirac point. Electron and holes are expected to have the same properties at the Dirac point. The orthogonal π and π^* do not interact, so the crossing of band-structure is possible. The yellow circle in Figure 10 shows the intersection of the valence band (VB) and conduction band (CB) clearer. Results show that graphene is a zerogap semiconductor because the VB and CB intersect at the Dirac point. Graphene's zero bandgap originates from the carbon-rich environment of the unit cell. In short, electron flow can happen at the top of the VB without any external stimulus, so electrons from the VB can flow into the CB at lower energy.

Graphene's outstanding electrical properties are due to its use of zero-mass, low-energy carriers that behave as relativistic Dirac fermions [55]. An independent energy-independent group velocity is seen in the low energy excitations of graphene's linear dispersion, meaning zero effective mass. Moreover, being massless allows an electron to quickly move within the graphene, which means graphene has high electron mobility. The difference in band structure for both monolayer and bilayer graphene is that monolayer graphene has a toroidal-like shape and exhibits a band state density that approaches zero at the Dirac point. Besides, the density

of states rises exponentially from zero energy with bilayer graphene, showing a hyperbolic band structure. Gapless band structure in AB-stacked bilayer graphene results in massive Dirac quasi-particles classified as Dirac Fermions in monolayer graphene [53].

Electron transfer from VB to CB is vital for current to flow. Therefore, electrical conductivity is heavily influenced by the bandgap of the material. In the absence of a semiconducting bandgap, semiconducting materials are impossible. This absence means that applications where graphene performs well, such as high-frequency analogue electronics and transparent conductive films, will be compromised. While silicon-based electronics dimensional scaling is approaching its limit, graphene semiconducting with a sizable bandgap might become the next generation's silicon alternative. Even though symmetry is commonly associated with geometry, it can also be disrupted through stacking two graphene layers in a Bernal stacking (AB stacking) [60]. Bilayer graphene sheets have two valence and conduction bands since they contain four atoms in a unit cell. Bilayer structure offers a new stacking order to fine-tune the electronic properties because of weak interlayer van der Waals interactions (forces). Consequently, modifying bilayer stacked graphene is suitable for fine-tunable electronic circuits or field-effect transistor (FET) applications. Bilayer graphene has been extremely promising since doping or an external electric field could open the energy gap [42,50]. Furthermore, applying external voltage and strain to bilayer graphene can increase the electron's mass [53].



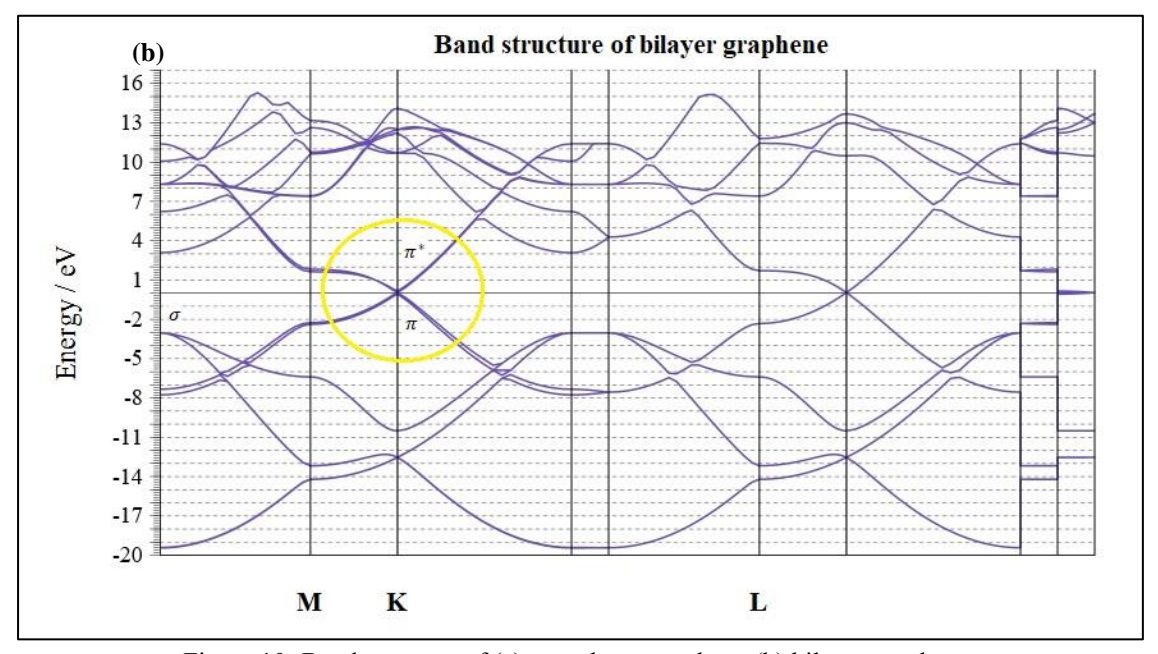


Figure 10. Band structure of (a) monolayer graphene (b) bilayer graphene

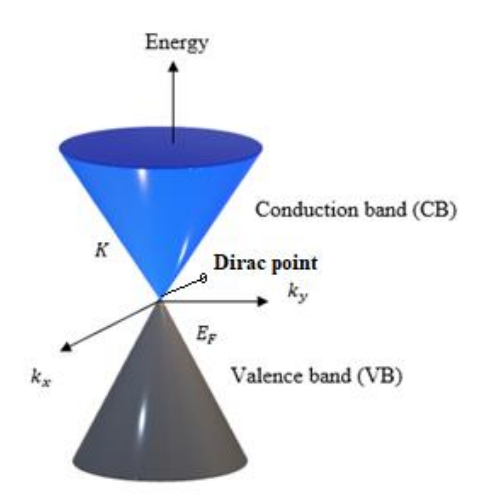


Figure 11. Dirac point band-structure of graphene

Conclusion

The Density Functional Theory (DFT) study involved a detailed theoretical investigation of monolayer and bilayer. Ultrasoft and norm-conserving pseudopotentials approaches were used in the calculations. Therefore, both Brillouin zone sampling parameters ($10 \times 10 \times 1$, k-point) and plane-wave monolayer and bilayer graphene parameters (320eV and 225eV, respectively) were optimized. The results of this study were computed using the open-source Quantum Espresso software package that incorporates the electronic structure software. Using the Broyden-Fletcher-Goldfarb-Shanno (BFGS) force and energy minimization method, monolayer and bilayer graphene were calculated to have a stable geometry. Graphene's very stable lattice and unit cell structure were discerned and observed using XCRYSDEN. The density of states and band gap have been calculated using the band calculation for groundstate properties. In both cases of graphene, zero DOS and 0eV for bandgap were recorded. Using this information, proving the properties of zero-gap semiconductor tags for graphene has been made possible. The shape of the band structure for monolayer graphene differs from bilayer graphene. hybridization of graphene is the same for monolayer and bilayer graphene but more time consuming for bilayer. Monolayer graphene is more stable molecularly than bilayer graphene due to having a larger (HOMO -LUMO) gap. Therefore, it is reasonable to assume that

results given by Quantum Espresso are reliable, given that the software has proven accurate in both electronic and structural analyses. At times, the absence of a zero-bandgap semiconductor material can hinder the use of electronic and optical devices. Expanding the study to AB stacked bilayer offers tremendous potential for application in devices due to its ability to tune the bandgap. The usage of graphene should not be restricted because it is a promising material. Stacking bilayer graphene with armchair and zigzag edges results in a bandgap value different from the bandgap obtained in this study. This subject is essential and requires more study from a theoretical and experimental perspective.

Acknowledgement

This work is funded by Short Term Grant with Project Code: 304/PFIZIK/6315241 for the financial supports, Research University Grant (RUI), USM (Grant code:1001/PFIZIK/8011113), and Fundamental Research Grant Scheme (FRGS) (Grant code: 203.PFIZIK.6711771).

References

1. Abbood, H. I. and Jabour, H. S. (2017). Theoretical study of electronic and electrical properties of pure and doped graphene sheets. *International Journal of Advanced Engineering Research and Science*, 4(7): 124-127.

- Arrigoni, M. and Madsen, G. K. H. (2018). Comparing the performance of LDA and GGA functionals in predicting the lattice thermal conductivity of semiconductor materials: the case of AlAs. Computational Materials Science, 156: 35 4-360.
- 3. Banerjee, S. and Bhattacharyya, D. (2008). Electronic properties of nano-graphene sheets calculated using quantum chemical DFT. *Computational Materials Science*, 44(1): 41-45.
- Bas, S. Z., Ozmen, M. and Yildiz, S. (2017). Electrochemical H₂O₂ sensor based on graphene oxide-iron oxide nanoparticles composite. 7th International Conference Nanomaterials: Application & Properties, pp. 04NB05-1.
- Castro, E. V, Peres, N. M. R., Santos, J. M. B. L. dos, Guinea, F. and Neto, A. H. C. (2008). Bilayer graphene: gap tunability and edge properties. *Journal of Physics: Conference Series*, 129: 012002.
- 6. Chaitanya Sagar, T. and Chinthapenta, V. (2018). Lower and upper bound estimates of material properties of pristine graphene: Using quantum espresso. *Advances in Structural Integrity* (pp. 253–265). Springer Singapore.
- 7. Chu, K.-L., Wang, Z.-B., Zhou, J.-J. and Jiang, H. (2017). Transport properties in monolayer–bilayer–monolayer graphene planar junctions. *Chinese Physics B*, 26(6): 067202.
- 8. Cooper, D. R., D'Anjou, B., Ghattamaneni, N., Harack, B., Hilke, M., Horth, A., Majlis, N., Massicotte, M., Vandsburger, L., Whiteway, E. and Yu, V. (2012). Experimental review of graphene. *ISRN Condensed Matter Physics*, 2012: 1-56.
- Cruz-Silva, E., Jia, X., Terrones, H., Sumpter, B. G., Terrones, M., Dresselhaus, M. S. and Meunier, V. (2013). Edge–Edge Interactions in Stacked Graphene Nanoplatelets. ACS Nano, 7(3): 2834-2841.
- Dai, X. S., Shen, T. and Liu, H. C. (2019). DFT study on electronic and optical properties of graphene modified by phosphorus. *Materials Research Express*, 6(8): 085635.
- 11. Dinh Le, T.-S., An, J. and Kim, Y.-J. (2017). Femtosecond laser direct writing of graphene oxide

- film on polydimethylsiloxane (PDMS) for flexible and stretchable electronics. *Conference on Lasers and Electro-Optics Pacific Rim (CLEO-PR)*, 2017: 1-4.
- Freitas, R. R. Q., Rivelino, R., Mota, F. de B. and de Castilho, C. M. C. (2011). DFT Studies of the Interactions of a Graphene Layer with Small Water Aggregates. *The Journal of Physical Chemistry A*, 115(44): 12348-12356.
- 13. Gao, H. and Liu, Z. (2017). DFT study of NO adsorption on pristine graphene. *RSC Advances*, 7(22): 13082-13091.
- 14. Geng, W., Zhao, X., Liu, H. and Yao, X. (2013). Influence of interface structure on the properties of ZnO/graphene composites: A theoretical study by density functional theory calculations. *The Journal* of *Physical Chemistry C*, 117(20): 10536-10544.
- Giannozzi, P., Baroni, S., Bonini, N., Calandra, M., Car, R., Cavazzoni, C., Ceresoli, D., Chiarotti, G. L., Cococcioni, M., Dabo, I., Dal Corso, A., de Gironcoli, S., Fabris, S., Fratesi, G., Gebauer, R., Gerstmann, U., Gougoussis, C., Kokalj, A., Lazzeri, M., ... and Wentzcovitch, R. M. (2009). Quantum Espresso: a modular and open-source software project for quantum simulations of materials. *Journal of Physics: Condensed Matter*, 21(39): 395502.
- Giannozzi, P., Baseggio, O., Bonfà, P., Brunato, D., Car, R., Carnimeo, I., Cavazzoni, C., de Gironcoli, S., Delugas, P., Ferrari Ruffino, F., Ferretti, A., Marzari, N., Timrov, I., Urru, A. and Baroni, S. (2020). Quantum Espresso toward the exascale. *The Journal of Chemical Physics*, 152(15): 154105.
- 17. Gil, D. M., Defonsi Lestard, M. E., Estévez-Hernández, O., Duque, J. and Reguera, E. (2015). Quantum chemical studies on molecular structure, spectroscopic (IR, Raman, UV–Vis), NBO and Homo–Lumo analysis of 1-benzyl-3-(2-furoyl) thiourea. Spectrochimica Acta Part A: Molecular and Biomolecular Spectroscopy, 145, 553-562.
- Gopinath, K. P., Vo, D.-V. N., Gnana Prakash, D., Adithya Joseph, A., Viswanathan, S. and Arun, J. (2021). Environmental applications of carbonbased materials: a review. *Environmental Chemistry Letters*, 19(1): 557-582.

- 19. Griffiths, K., Dale, C., Hedley, J., Kowal, M. D., Kaner, R. B. and Keegan, N. (2014). Laser-scribed graphene presents an opportunity to print a new generation of disposable electrochemical sensors. *Nanoscale*, 6(22): 13613–13622.
- Hossain, M. T., Alam, M. N. K. and Islam, M. R. (2016). Gate oxide dependent performance of graphene FET using quasi-ballistic transport model.
 3rd International Conference on Electrical Engineering and Information Communication Technology (ICEEICT), pp. 1-5.
- Hosseindokht, Z., Paryavi, M., Asadian, E., Mohammadpour, R., Rafii-Tabar, H. and Sasanpour, P. (2017). Pressure sensor based on patterned laser scribed reduced graphene oxide; experiment & modeling. 2017 International Conference on Orange Technologies (ICOT), pp. 15-17.
- 22. Jeon, C., Shin, H.-C., Song, I., Kim, M., Park, J.-H., Nam, J., Oh, D.-H., Woo, S., Hwang, C.-C., Park, C.-Y. and Ahn, J. R. (2013). Opening and reversible control of a wide energy gap in uniform monolayer graphene. *Scientific Reports*, 3(1): 2725.
- 23. Jigmat Stondus. (2016). Study of single and fewlayers MoS₂ crystals. Master of Science, Banaras Hindu University.
- 24. Ke, X., Hao, G., Rong, Y., Zhou, X., Liu, J., Xiao, L. and Jiang, W. (2016). A facile approach to the hydrothermal synthesis of graphene. 16th International Conference on Nanotechnology (IEEE-NANO), pp. 604-607.
- 25. Koay, H. W., Ruslinda, A. R., Hashwan, S. S. B., Fatin, M. F., Thivina, V., Tony, V. C. S., Md Arshad, M. K., Voon, C. H. and Hashim, U. (2016). Surface morphology of reduced graphene oxide-carbon nanotubes hybrid film for bio-sensing applications. *International Conference on Semiconductor Electronics (ICSE)*, pp. 320-323.
- 26. Kumar, R., Dias, W., Rubira, R. J. G., Alaferdov, A. V., Vaz, A. R., Singh, R. K., Teixeira, S. R., Constantino, C. J. L. and Moshkalev, S. A. (2018). Simple and fast approach for synthesis of reduced graphene oxide–MoS₂ hybrids for room temperature gas detection. *IEEE Transactions on Electron Devices*, 65(9): 3943-3949.
- 27. Lebedeva, I. V., Knizhnik, A. A., Popov, A. M.,

- Lozovik, Y. E. and Potapkin, B. V. (2011). Interlayer interaction and relative vibrations of bilayer graphene. *Physical Chemistry Chemical Physics*, 13(13): 5687.
- 28. Lin, S.-P., Ciou, J.-Y., Lai, T.-Y. and Lin, T.-W. (2017). Impedimetric investigation of dual electrical properties of reduced graphene-oxide-based biosensors in the detection of dopamine. 39th Annual International Conference of the IEEE Engineering in Medicine and Biology Society (EMBC), pp. 4098-4101.
- 29. Liu, X.-S., Bo, Z.-M., Tu, W.-C., Lin, M.-Y. and Chen, S.-L. (2017). Enhanced performance of reduced graphene oxide photodetectors by Ag nanoparticles. *Eleventh International Conference on Sensing Technology (ICST)*, pp. 1-4.
- 30. Liu, Z., Suenaga, K., Harris, P. J. F. and Iijima, S. (2009). Open and closed edges of graphene layers. *Physical Review Letters*, 102(1): 015501.
- 31. Marguna, S., Sulthoni, M. A., Anshori, I., Yuliarto, B., Surawijaya, A. and Utari, L. (2019). Synthesis of zinc oxide (ZnO) graphene nanocomposite as CO gas sensor application. *International Symposium on Electronics and Smart Devices* (ISESD), pp. 1-4.
- 32. Mi, W.-T., Qi, H.-Y., Zhao, H.-M., Li, Y.-X., Yang, Y. and Ren, T.-L. (2016). Ultrasound-aided spray casting for graphene oxide deposition. 2016 IEEE International Nanoelectronics Conference (INEC), pp. 1-2.
- 33. Mucha-Kruczyński, M., Aleiner, I. L. and Fal'ko, V. I. (2011). Strained bilayer graphene: Band structure topology and Landau level spectrum. *Physical Review B*, 84(4): 041404.
- 34. Ng, W.-B. (2018). Graphene-based materials for biotransistor application. Doctoral thesis, Nanyang Technological University, Singapore.
- 35. Ojo, O. O., Jonnalagadda, S. B. and Martincigh, B. S. (2018). Synthesis of graphene oxide under differing conditions and its characterization. 8th International Conference Nanomaterials: Application & Properties (NAP), pp. 1-4.
- 36. Pang, Y., Yang, Z., Xie, X. and Tao, L.-Q. (2020). Graphene oxide modified porous graphene for aqueous alcohol detection. *IEEE Sensors Letters*, 4(2): 1-4.

- Papadakis, I., Stathis, A., Karampitsos, N., Stavrou, M., Kyrginas, D. and Couris, S. (2020). UV Laser photo-reduction of graphene oxide and graphene fluoride for the efficient tuning of their nonlinear optical response. 22nd International Conference on Transparent Optical Networks (ICTON), pp. 1-4.
- 38. Pashangpour, M. and Ghaffari, V. (2013). Investigation of structural and electronic transport properties of graphene and graphane using maximally localized Wannier functions. *Journal of Theoretical and Applied Physics*, 7(1): 9.
- Quhe, R., Ma, J., Zeng, Z., Tang, K., Zheng, J., Wang, Y., Ni, Z., Wang, L., Gao, Z., Shi, J. and Lu, J. (2013). Tunable band gap in few-layer graphene by surface adsorption. *Scientific Reports*, 3(1): 1794.
- 40. Rai, S., Bhujel, R. and Swain, B. P. (2018). Electrochemical analysis of graphene oxide and reduced graphene oxide for super capacitor applications. *IEEE Electron Devices Kolkata Conference (EDKCON)*, pp. 489-492.
- 41. Rana, S., Sandhu, I. S. and Chitkara, M. (2018). Exfoliation of graphene oxide via chemical reduction method. 6th Edition of International Conference on Wireless Networks & Embedded Systems (WECON), pp. 54-57.
- 42. Rani, P. and Bhandari, R. (2013). DFT study of defects in graphene. *International Conference on Advanced Nanomaterials & Emerging Engineering Technologies*, pp. 237-239.
- 43. Rani, P., Dubey, G. S. and Jindal, V. K. (2014). DFT study of optical properties of pure and doped graphene. *Physica E: Low-Dimensional Systems and Nanostructures*, 62: 28-35.
- Razado-Colambo, I., Avila, J., Vignaud, D., Godey, S., Wallart, X., Woodruff, D. P. and Asensio, M. C. (2018). Structural determination of bilayer graphene on SiC(0001) using synchrotron radiation photoelectron diffraction. *Scientific Reports*, 8(1): 10190.
- Rozhkov, A. V., Sboychakov, A. O., Rakhmanov, A. L. and Nori, F. (2016). Electronic properties of graphene-based bilayer systems. *Physics Reports*, 648: 1-104.

- 46. Ayyappan, S. & R.Nithya. (2018). Molecular structure, NBO and HOMO-LUMO analysis of quercetin on single layer graphene by density functional theory. *Digest Journal of Nanomaterials and Biostructures*, *13*(1): 97-105.
- 47. Seenithurai, S., Pandyan, R. K., Kumar, S. V., & Mahendran, M. (2013). Electronic Properties of boron and nitrogen doped graphene. *Nano Hybrids*, 5: 65-83.
- Shruthi, G., Anshika, Baishali, G., Nella, N., Radhakrishna, V. and Rajanna, K. (2018). Investigation on reduced graphene oxide for radiation sensing application. *IEEE Sensors*, pp. 1-4.
- 49. Song, S., Zhao, H., Zheng, X., Zhang, H., Liu, Y., Wang, Y. and Han, B. (2018). A density functional theory study of the role of functionalized graphene particles as effective additives in power cable insulation. *Royal Society Open Science*, 5(2): 170772.
- 50. Khan, T. T. (2017). Spectroscopic and microscopic analysis of graphene for sensor applications. The U niversity of Texas at El Paso.
- 51. Tencha, A., Fedoriv, V., Shtepliuk, I., Yakimova, R., Ivanov, I., Khranovskyy, V., Shavanova, K. and Ruban, Y. (2017). Synthesis of graphene oxide inks for printed electronics. *IEEE International Young Scientists Forum on Applied Physics and Engineering (YSF)*, pp. 155-158.
- 52. Thema, F. T., Moloto, M. J., Dikio, E. D., Nyangiwe, N. N., Kotsedi, L., Maaza, M. and Khenfouch, M. (2013). Synthesis and characterization of graphene thin films by chemical reduction of exfoliated and intercalated graphite oxide. *Journal of Chemistry*, 2013: 1-6.
- Torrisi, L., Silipigni, L. and Cutroneo, M. (2018).
 Radiation effects of IR laser on graphene oxide irradiated in vacuum and in air. *Vacuum*, 153: 122-131.
- 54. You, T., Yang, N., Shu, Y. and Yin, P. (2019). A DFT study on graphene-based surface-enhanced Raman spectroscopy of Benzenedithiol adsorbed on gold/graphene. *Journal of Raman Spectroscopy*, 50(10): 1510-1518.

Nurhafizah et al.: DFT STUDY ON STRUCTURAL PROPERTIES, DENSITY OF STATES AND BAND STRUCTURE OF MONOLAYER & BILAYER GRAPHENE

- 55. Zainal, N., How, J. F., Choo, X. H. and Soon, C. F. (2020). Synthesis and characterization of graphene oxide (GO) and reduced graphene oxide (rGO) using Modified Tour's method for sensing device applications. 2020 IEEE Student Conference on Research and Development (SCOReD): pp. 385-390.
- Zhan, D. (2013). Structural and electronic properties of graphene and modified graphene. Doctoral thesis, Nanyang Technological University, Singapore.
- 57. Zhang, D., Liu, J. and Xia, B. (2016). Layer-by-layer self-assembly of zinc oxide/graphene oxide hybrid toward ultrasensitive humidity sensing. *IEEE Electron Device Letters*, *37*(7): 916-919.
- 58. Zhang, Y., Tang, T.-T., Girit, C., Hao, Z., Martin, M. C., Zettl, A., Crommie, M. F., Shen, Y. R. and Wang,

- F. (2009). Direct observation of a widely tunable bandgap in bilayer graphene. *Nature*, 459(7248): 820-823.
- 59. Vu, K. B., Le Phuc Nhi, T., Vu, V. V. and Tung Ngo, S. (2020). How do magnetic, structural, and electronic criteria of aromaticity relate to HOMO – LUMO gap? An evaluation for graphene quantum dot and its derivatives. *Chemical Physics*, 539: 110951.
- 60. Zhu, Z., Chutia, A., Sahnoun, R., Koyama, M., Tsuboi, H., Hatakeyama, N., Endou, A., Takaba, H., Kubo, M., Del Carpio, C. A. and Miyamoto, A. (2008). Theoretical study on electronic and electrical properties of nanostructural ZnO. *Japanese Journal of Applied Physics*, 47(4): 2999-3006.